Petrogeochemistry of the Sungun Porphyry Copper Intrusive Rocks, Azerbaijan, Iran

A. Hezarkhania
Assistant Professor
Department of Mining, Metallurgy and Petroleum Engineering,
Amirkabir University of Technology

Abstract

Based on the petrographical and petrochemical studies, it is suggested that the Sungun deposit as a composite stock, emplaced at a paleo-depth of ~2000 m, and comprising early monzonite/quartz-monzonite and a later diorite/granodiorite phase. The parental magma was a medium to high K andesite or diorite, initially contained >3 wt percent H_2O (wet magma), and generated in continental arc settings. The high level emplacement of this magma, led to its saturation with water and the exsolution of fluids at an early stage of crystallization, and subsequently Mo and then Cu mineralization in the stock. Based on the major and trace element geochemistry, especially the behaviour of the immobile trace elements, Y, Zr and Nb, the fractional crystallization is suggested for the petrological characteristics of the present intrusive rocks. The degree of fractionation was estimated using a Rayleigh fractionation equation, which related the concentration of Zr, Nb and Y in the least altered sample to their concentrations in progressively more evolved samples. The results of these calculations indicated that the compositions of the various rock types can be explained by up to 24 % fractionation of a dioritic or andesitic magma to produce the more evolved monzonite/quartz-monzonite suite and chemically altered diorite-granodiorite suite.

Keywords

Petrogeochemistry, Copper, Porphyry, Iran.

Introduction

The Sungun porphyry copper deposit is one of two major copper deposits associated with calc-alkaline intrusive rocks (stocks) in the Cenozoic Sahand-Bazman volcanic belt, which extends north-westward from Sahand volcano in Azarbaijan province, to the Bazman volcano in south-east Iran, a distance of approximately 1700 km. This belt, which was first identified by Stöcline (1977), consists of alkaline and calc-alkaline volcanic rocks (Fig. 1), and related intrusives (I-type) and was formed by subduction of the Arabian plate beneath central Iran during the Alpine orogeny [1, 2, 3, 43, 46, 47].

The oldest rocks in the Sungun area are Upper Cretaceous carbonate rocks and are overlain disconformably by Eocene basic volcanics and sandstones. In the Early to Middle Tertiary (Eocene to Miocene), a major episode of volcanism, plutonism, and deformation occurred in the Sahand-Bazman belt. In the Sungun area, magmatism was initiated by eruption of Eocene volcanic rocks, which continued to Upper Miocene time. The composition of these rocks varies from andesite to rhyolite. Associated intrusive rocks comprise mainly granodiorite, granite and monzonite. This episode was an expression of Andean-type magmatism that developed along the continental margin in response to subduction tectonics to the north [2, 3].

This paper addresses some unresolved questions on the petrology, petrochemistry and petrogenesis of the Sungun stock. The emphasis is on the evolution of the magma, which is modelled using the composition of the rocks that comprise the stock, and a variety of other geological data including the results of mapping, drill core logging, petrography, and mineral chemical analyses. Petrographic studies were carried out on 60 thin and polished thin sections of the freshest rocks; 14 of them were selected for electron microprobe analyses, and the results are presented in (Table 1). Twenty whole rock samples were analyzed for major and trace elements using X-ray fluorescence (XRF), and the results are in (Table 2). Some whole-rock geochemical data were supplemented by analyses from [34].

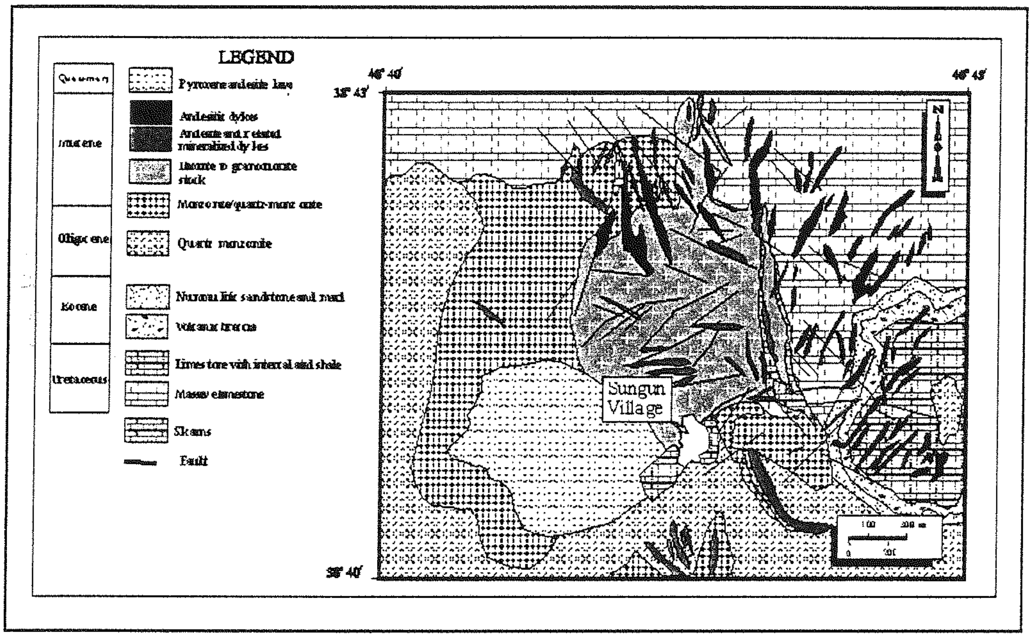

Figure (1) A geological map of the Sungun deposit, showing the field relationships among the various phases of the Sungun intrusion, and the country rocks. The major intrusive bodies are monzonite/quartz-monzonite in the west and later diorite/granodiorite in the east. Both these units are bounded to the north and east by Cretaceous limestone. Andesitic to dacitic dykes are distributed mostly in the north and western parts of the Sungun deposit (outside the main stock). Mineralized trachyandesitic dykes occur mainly within the diorite/granodiorite and less commonly in the quartz-monzonite. Skarn-type alteration (and associated mineralization) occurs as a narrow rim along the eastern and northern margin of the stock in the Sungun valley, [27, 34].

Geological Setting

The Sungun intrusive complex is located about 75 km north-west of Ahar (north-western Iran), in Azarbaijan province in north-western Iran, and intruded along the Sungun anticline into Cretaceous limestone and Eocene tuff (equivalent to the Karaj formation) and agglomerate of andesitic to trachytic composition. To the north and east, the stock is bounded by hydrothermally altered Cretaceous limestone (skarn), which contains economic copper mineralization [18, 19, 23, 24, 25].

The oldest rocks exposed in the study area are a ~500 m sequence of Cretaceous limestone with intercalations of shale, and a ~1500 m thick sequence of Middle to early Late Tertiary, intermediate composition, calc-alkaline volcanic, and tuffaceous rocks intruded by numerous calc-alkaline dykes. The entire stock and volcanic "cover rocks" are located within a caldera. Geological relations in the

Sungun area have been interpreted from more than 20,000 m of drill core made available by the Ahar Copper Company. The stock has a plan area of approximately 3.45 km^2 (1.5 x 2.3 km), (elongated NW-SE), and consists of three different intrusive phases. Almost all intrusive units contain the same assemblage of minerals: plagioclase, K-feldspar, quartz, biotite, hornblende (which is typically altered to biotite and/or chlorite), titanite, rutile, scheelite, apatite, minor magnetite, and zircon. The intrusives at Sungun are 1) monzonite/quartz-monzonite; 2) diorite/granodiorite; and 3) andesitic and related dykes, in order of emplacement (Fig. 1). Monzonite/quartz-monzonite are mainly porphyritic, and exposed to the west of the diorite/granodiorite intrusion, and in a small body in the southeast. Diorite/granodiorite forms the central part of the Sungun stock and intrudes monzonite/quartz-monzonite. All the intrusives are generally unfoliated and commonly porphyritic, suggesting a shallow level of emplacement [7]. The latter interpretation is supported by a stratigraphic reconstruction, which shows that the maximum depth of intrusion was 2000 m.

Rocks in the study area were subjected to intense hydrothermal alteration, especially within and adjacent to the diorite/granodiorite intrusive [19, 20, 21, 23]. Petrographically, fresh rocks were only available for sampling at depths >500 m below the present erosional surface. Even in the outermost part of the area, it is not possible to find completely fresh igneous rocks in outcrop. Several stages of hydrothermal alteration and associated mineralization have produced new minerals, created new textural relationships and in many cases obliterated the primary character of the rock.

Petrography

Monzonite and quartz-monzonite

Monzonite and quartz-monzonite are light grey in colour and contain phenocrysts of K-feldspar, plagioclase, biotite and hornblende in a fine-grained matrix. The contact between monzonite and the adjacent quartz-monzonite is gradual, and chemical analyses show that these two rock types are chemically the same, but different in terms of texture (discussed later).

The monzonite/quartz-monzonite intrusives can be distinguished from the other units by the presence of up to 30 volume percent of euhedral to subhedral tabular plagioclase phenocrysts (25 - 40 vol. %), euhedral K-feldspar (occupying more than 15 vol. %), euhedral to subhedral biotite phenocrysts (up to 10 vol. %), hornblende phenocrysts, ($\leq$2 vol. %), and anhedral to highly corroded quartz phenocrysts (up to ~20 vol. %). The groundmass consists mainly of quartz, K-feldspar and plagioclase (An_{1-25}). Quartz in the groundmass is mostly interstitial and commonly contains biotite and muscovite inclusions, which show that it formed late. The groundmass coarsens and the phenocrysts increase in size with increasing depth and distance from wall rock contacts.

In shallow exposures, plagioclase phenocrysts (up to 5 mm in diameter) are, euhedral and normally zoned (An_{40-15}), partially resorbed tabular crystals, which have strongly sericitized, calcic-bearing cores (An_{40-25}). According to [49], this type of alteration in plagioclase is consistent with the early crystallization of an anorthitic core which becomes unstable on cooling and subsequently alters to sericite and calcite. There are two types of K-feldspar; phenocrysts, up to 20 mm in diameter, containing euhedral to subhedral inclusions of plagioclase (An_{40-15}) and biotite, and K-feldspar pseudomorphs (up to 10 mm in diameter) which replaced plagioclase phenocrysts. Biotite phenocrysts are up to 3 mm in diameter and have been altered to chlorite and sericite at shallow depths in the pluton. Hornblende (up to 9 mm in diameter) displays blue to pale green pleochroism of variable intensity and, twinning, and has a composition intermediate between magnesio-hornblende and edenitic hornblende (based on the [40]). Augite has been reported to occur at depth in the monzonite/quartz-monzonite by [34] but was not observed during the present study. Based on textural relationships the sequence of crystallization of phenocryst phases was plagioclase and K-feldspar, follow by biotite and rare hornblende.

Accessory minerals include titanite, apatite, zircon, rutile, magnetite, ilmenite, monazite, scheelite, and uraninite which occur randomly, both in the silicate phases and interstitial to them. Titanite is more abundant than the other accessories, and forms anhedral grains intergrown with magnetite and rutile. Ilmenite forms sparse isolated grains locally rimmed by titanite. The sulphide minerals are rare and consist of pyrite and traces of chalcopyrite, galena and sphalerite. Together with chlorite, they replace biotite or occur interstitially to quartz and feldspar in the groundmass.

Diorite/granodiorite

Diorite/granodiorite is porphyritic, and ranges from fine-grained in the northern part to coarse-grained in the west and northwest, where it intrudes monzonite to quartz-monzonite (Fig. 2). Dark green xenoliths (up to 12 cm in diameter) consisting of hornblende, biotite (which impart the colour), and plagioclase phenocrysts set in a fine-grained groundmass of quartz and feldspar are common in the outer parts of the diorite/granodiorite intrusion (discussed later). The contact with the monzonite/quartz-monzonite is not well exposed, and, where seen, is commonly brecciated. A feature of the porphyritic diorite/granodiorite is that it contains numerous mineralized dykes. The contact between granodioritic rocks and Cretaceous limestone is well exposed in the northern and eastern parts of the study area. In the east the latter has been altered to skarn which locally contains abundant copper mineralization.

Phenocrysts comprise about 50 percent by volume of the rock and are represented mainly by plagioclase up to 4 mm in diameter (~30 vol. %), K-feldspar up to 20 mm in diameter (~10 vol. %), amphibole up to 5 mm in diameter (~10 vol. %) quartz up to 2 mm in diameter (~7 vol. %) and biotite up to 4 mm in diameter (<3 vol. %). The amphibole has a composition intermediate between magnesio-hornblende and edenitic hornblende (based on the classification of [40]. Except at depth, it has been completely replaced by biotite and is only recognizable from the characteristic amphibole morphology of psodomorphs and in some cases rutile needles alligned in the direction of the principal cleavages. Textural relationships show that plagioclase and K-feldspar phenocrysts formed shortly after amphibole phenocrysts, and that quartz and biotite phenocrysts formed during the last stage of magma crystallization. Quartz phenocrysts are anhedral and rarely contain biotite and muscovite inclusions.

Most of the plagioclase phenocrysts have been altered to sericite, quartz, calcite, and gypsum. Based on petrography and electron microprobe analyses, two generations of plagioclase are distinguishable in terms of size, inclusions, and composition; large crystals (phenocrysts) with highly altered cores and relatively small crystals with clear carlsbad twinning (An_{1-5}), that are interpreted to have formed during a sodic alteration episode, because of the compositional similarity to the albitic rims around K-feldspar which were clearly developed during sodic alteration [20, 21, 22]. Plagioclase phenocrysts range in composition from oligoclase-andesine in the core (An_{15-32}) to albite (An_{1-5}) at the rim [23, 24, 25].

Petrographic observations and microprobe analyses also indicate the presence of two compositionally distinguishable types of K-feldspar within this rock unit, I) phenocryst, and II) hydrothermal K-feldspar. K-feldspar phenocrysts are mainly anhedral, small in size (<3 mm) and perthitic ($Or_{97}Ab_2An_1$ to $Or_{99}Ab_1$ and $Ab_{76}Or_1An_{23}$ to $Ab_{81}Or_3An_{16}$) and contain up to 1.7 wt % BaO. They commonly contain small inclusions of primary biotite, plagioclase, and the accessory minerals, apatite, titanite, and zircon. Hydrothermal K-feldspar may be distinguished from magmatic K-feldspar by the absence of perthitic intergrowths.

The biotite phenocrysts are brown, up to 3 mm in diameter, Fe-enriched and subhedral.

Pale-brown to greenish-brown, Mg-enriched, biotite forms small ragged crystals interpreted to be of hydrothermal origin.

Quartz phenocrysts in this suite are commonly rounded, suggesting that pressures fluctuated during crystallization [51, 52, 53, 54]. The presence of hornblende as phenocrysts, in the freshest samples in deep part of the stock (i.e. an early liquidus phase) indicates that the granodioritic magma contained >3 wt percent H_2O, which led to water saturation during early crystallization [4, 53, 54]. The latter could be the reason that the diorite was potentially able to alter the Cretaceous carbonate rocks to skarn at the contact.

Accessory minerals are apatite, zircon, rutile, titanite, ilmenite, monazite, scheelite and uraninite in order of abundance. These minerals occur both in the silicate phases (i.e., biotite, plagioclase and K-feldspar) and interstitial to them (in the groundmass). The sulphide minerals consist of pyrite, chalcopyrite, molybdenite, argento-pentlandite, a silver telluride (hessite), galena, and sphalerite and occur as inclusions in altered biotite or interstitially in the matrix of the rock.

As mentioned before, diorite/granodiorite contains mafic rounded xenoliths. They are fine- to medium-grained, and contain green hornblende (1 mm long, and 5 vol. %), biotite (>1 mm in diameter, and ~8 vol. %), and plagioclase (An_{10-28}, and 30 vol. %) phenocrysts. Accessory minerals are apatite (euhedral), zircon (euhedral to anhedral), magnetite (euhedral to subhedral) and titanite (subhedral to anhedral). The groundmass is microcrystalline, and is formed mainly from quartz and feldspar. The hornblende occurs as ragged laths, or as irregularly distributed subhedral to euhedral phenocrysts. Crystal rims have been altered to biotite, magnetite, and plagioclase. Along the margins of the xenoliths, there are concentrations of ragged grains of biotite, suggesting the reaction of hornblende to biotite.

Based on the mineralogical and petrographic similarity of the xenoliths to diorite, the xenoliths are interpreted to have formed by stoping of earlier crystallized material during ascent of later pulses of magma. A small proportion of xenoliths consists of green to greenish brown pyroclastic rocks and tuffs. They contain plagioclase (An_{35-20}), broken quartz and opaque minerals, in a fine-grained matrix of quartz, chlorite and feldspar (mainly plagioclase).

Dykes

Two types of dyke crosscut the granodiorite, I) light-brown highly altered and mineralized andesitic dykes, up to 2 m thick (called mineralized dykes in Figure 2), II) dark-brown almost fresh and unmineralized andesitic dykes, up to 4 m thick. The phenocryst phases in the mineralized dykes are plagioclase, K-feldspar, quartz, biotite and hornblende. The phenocryst/groundmass ratio is approximately one. The groundmass consists mainly of quartz and feldspar. Biotite and hornblende phenocrysts are altered to chlorite, and feldspars are altered to sericite. Accessory minerals consist of titanite and lesser magnetite. Sulphide minerals in mineralized dykes consist mainly of pyrite (up to 10 vol. %) and chalcopyrite (<1 vol. %). A conspicuous feature of these dykes is the presence of spherically shaped secondary magnetite. These spheres are thought to represent replacement of precursor pyrite. Unmineralized dykes contain biotite, amphibole (magnesio-hornblende), and zoned euhedral plagioclase (from An_{10-15} to An_{15-35}) phenocrysts. The proportion of phenocrysts to groundmass is 1:3. One of the characteristics of unmineralized dykes is the absence of K-feldspar. These dykes belong to the youngest phase of granodioritic-related igneous activity, and cut both monzonite/quartz-monzonite in the north and diorite/granodiorite in the centre of the stock (Fig. 2).

Major and Trace ElementL Geochemistry

Representative samples of least altered diorite/granodiorite, monzonite/quartz-monzonite, andesite and mineralized dykes were analyzed for major and trace element compositions. All samples were analyzed by XRF techniques in the Geochemistry Laboratory, McGill University, except for six samples which were analysed for REE using the neutron activation method at ACTLABS Ontario (Table 3). Thirty whole rock analyses of the igneous rock, reported by [34] were incorporated in the data base. Hydrothermal alteration affected all the rock units, and caused re-distribution/mobilization of the alkali elements (e.g., K, Na and Sr) and silica (added as silicification) in almost all rock types [21, 22, 23, 24, 35, 36].

The classifications of [55] and [8, 9] show that the Sungun igneous rocks are mainly in the range of trachyandesite to andesite. They are also classified as syncollisional medium to high K, calc-alkaline rocks, which are generated from partial melting of basalt in continental arc settings (Fig 2). There is a clear petrochemical similarity between the Sungun igneous rocks and calc-alkaline rocks elsewhere in the Sahand-Bazman belt (Pourhosseini, 1982; 25, 16].

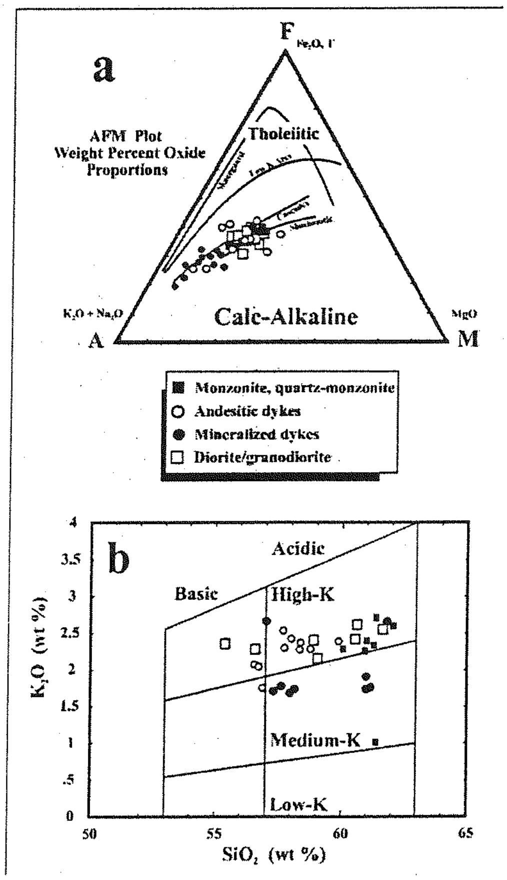

Figure (2) a. AFM plot of analyses of the Sungun stock. Skaergaard (tholeiitic) and Cascade (calc-alkaline) trends are from [5, 6] the Sungun intrusive rocks delineate a calc-alkaline trend. Trends of low K arc and shoshonitic volcanic suites are from [13]. b. K_2O (wt %) vs. SiO_2 (wt %) diagram showing the classification of [14, 15]. The Sungun intrusive rocks are classified as medium to high K andesite.

The different intrusives making up the Sungun stock have compositions which define a single linear trend on Harker diagrams for several major element oxides, suggesting a common source for and evolution of their magmas. Figure 3 show that MgO, CaO, MnO, Fe_2O_3 and TiO_2 decrease with increasing SiO_2. These negative trends are consistent with fractional crystallization of ferromagnesian minerals like hornblende (discussed later). Trends of increasing alkalis (Na and K) with increasing SiO_2 are also consistent with such fractionation (crystallization of progressively more sodic plagioclase and of K-feldspar), although the possibility that they also partly represent the effects of potassic and sodic alteration and silicification can not be excluded. Similar trends have been reported for porphyry copper deposits elsewhere [10, 11, 12, 13, 30, 31, 32]. Aluminum is highly immobile in porphyry copper deposits (Grant, 1986), and displays the same behaviour at Sungun, i.e., it shows as systematic variation with SiO_2.

The behaviour of a number of trace elements with increasing SiO_2 leads to the same conclusion as with many of the major elements, i.e., that variations in the primary compositions of the Sungun intrusives were the result of fractional crystallization. The decreasing trends for Ni (which substitute for Fe or Mg in hornblende) and Sr (which substitutes for Ca in hornblende and plagioclase) are consistent with their compatibility in early crystallizing minerals. Similarly the increasing trend of Rb, which substitutes for K, is consistent with the late crystallization of K-feldspar and biotite. The compatible trace elements Sc and Y and incompatible trace elements La, Zr, Nb and Th, as expected, also display negative and positive trends with SiO_2, respectively. The above notwithstanding, not all elements exhibit behaviour that can be explained by fractional crystallization. Chromium, shows a positive trend with increasing SiO_2. This is very unexpected as chromite is generally a very early liquidus phase and Cr is typically concentrated in mafic and ultramafic rocks. A possible explanation for the behaviour of Cr is that it did not saturate in the magma and because of its high charge/radius ratio behaved incompatibly.

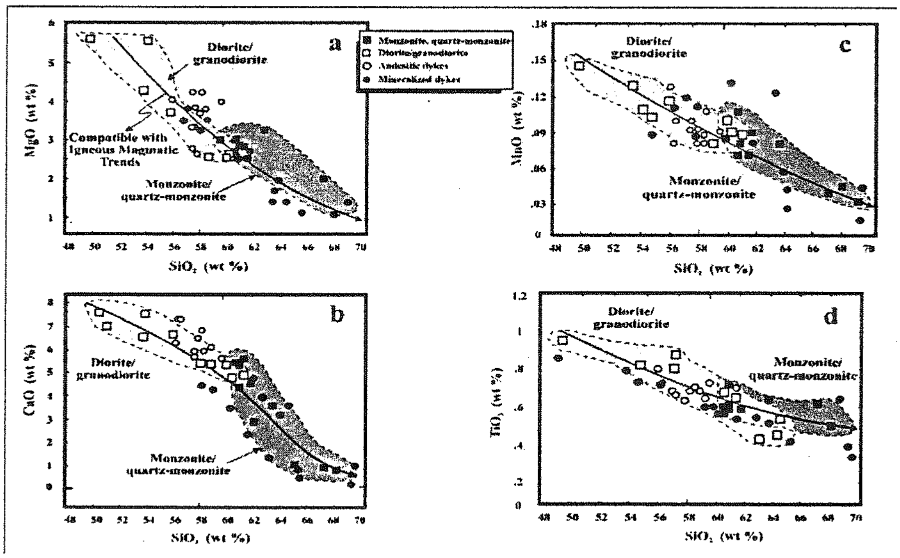

Figure (3) Harker diagram for the different suites of intrusive rocks at Sungun. a. MgO vs. SiO_2, b. CaO vs. SiO_2, c. MnO vs SiO_2 and d. TiO_2 vs. SiO_2. All diagrams have negative trends, which is consistent with the evolution of the corresponding magma(s) by fractional crystallization of minerals like hornblende and Ca-plagioclase. Possible fractionation curves are indicated by least square polynomial fits to the data (solid lines). The dark and light shaded fields correspond to the monzonite/quartz-monzonite and diorite/granodiorite fields, respectively.

Somewhat surprisingly, however, the more evolved monzonite/quartz-monzonite suite was intruded before the less evolved diorite/granodiorite suite, which hosts the bulk of the mineralization. In most cases the fields for these suites overlap. This and their co-linearity suggest that the two suites crystallized from the same magma. However, in several cases, notably for Co vs. SiO_2 and Sc vs. SiO_2, the fields are quite separate which may indicate separate magmas. This could, in turn, help explain why the more evolved phase of the pluton was introduced earlier. The late unmineralized andesite dykes generally plot in the same field as the main diorite/granodiorite intrusion, which is consistent with both units having crystallized from the same magma. By contrast the mineralized dykes plot in both fields and more commonly in the monzonite/quartz-monzonite field. This may indicate that the mineralized dykes have a different affinity to the unmineralized dykes. More probably, however, the data distribution is an artifact of alteration. Figure 4, shows the tectonic settings of the different rock types within the Sungun porphyry system.

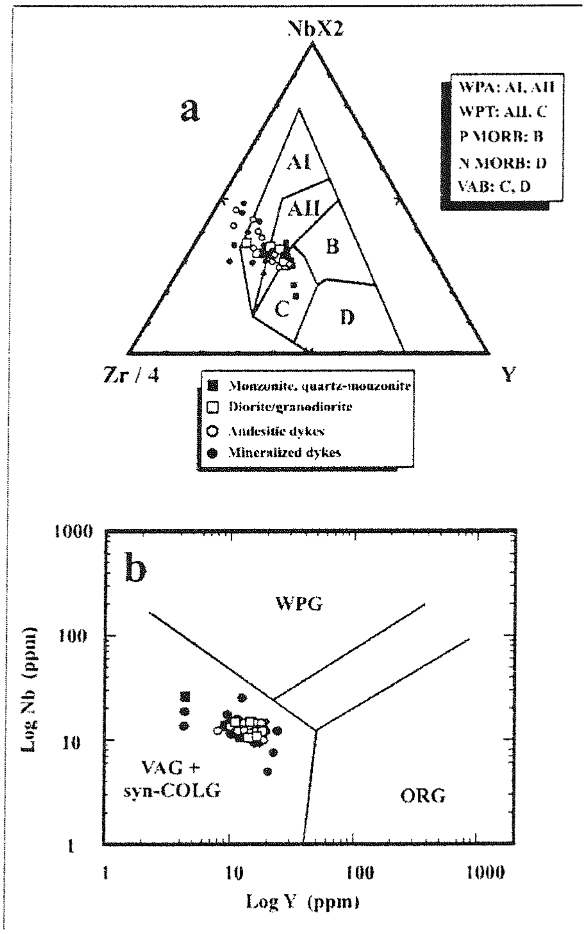

Figure (4) a. Nb * 2, Zr/4, Y diagram showing the tectonic setting (within plate arc) of different rock suites in the Sungun deposit, diagram after [41, 42], b. LogNb vs. logY, which shows that all the rock types in the Sungun stock fall in the volcanic arc felsic field Diagram after Meschede (1986). Abbreviations; WPA = within plate arcs, WPT = within plate tholeiites, P MORB = primitive mid-ocean ridge basalts, N MORB = normal mid-ocean ridge basalts, VAB = volcanic arc basalts, WPG = within plate granites, VAG = volcanic arc granites, ORG = ocean ridge granites.

All the Sungun intrusive rock types have similar distributions on chondrite-normalized spider diagrams, characterized by strong enrichment in most incompatible elements and depletion in compatible elements (Fig. 5). These distributions are important feature of calc-alkaline arc magmatism [8, 9]. Generally diorite/granodiorite is more enriched in compatible than monzonite/quartz-monzonite, and vice versa in respect to incompatible elements.

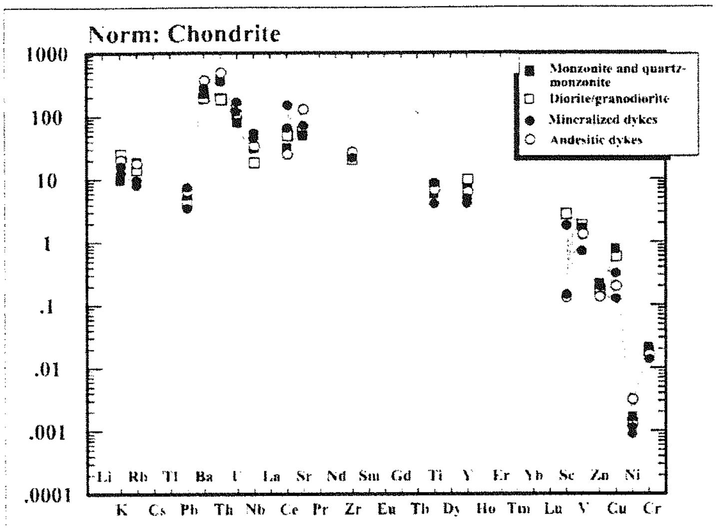

Figure (5) A Chondrite-normalized trace element spider diagram showing the compositions of the different intrusive suites in the Sungun stock. All suites display strong enrichment in most incompatible elements (low field strength elements, e.g. Ba, Sr, Ce, U, and Th) relative to chondrite, and depletion in compatible elements which is an important characteristic of calc-alkaline arc magmatism. They are also depleted in some high field strength elements e.g. P, V and Y. Chondrite normalization factors are from [33].

Chondrite-normalized rare earth element diagrams for the monzonite/quartz-monzonite and diorite/granodiorite show that these rocks are enriched in both compatible and incompatible REE's relative to Chondrite (Fig. 6 and Table 3). The rocks are characterized by LREE enrichment ($La/Yb_{(N)} > 30$) and lack a Eu anomaly. Monzonite/quartz-monzonite is more enriched in LREE and depleted in HREE than diorite/granodiorite or andesite, whereas diorite/granodiorite andesite, and mineralized dykes have similar profiles which is consistent with their crystallization from the same magma. The profiles for the various units fall within the range of typical calc-alkaline magmas (low SiO_2 and high SiO_2 andesites) generated in subduction zones [26].

P-T ConcitionsO of Crystallization

As discussed in [20, 24] it has been estimated the pressure of emplacement of the stock to be ~500 bars from stratigraphic reconstruction. This pressure corresponds to the lower-pressure limit of stability of the assemblage plagioclase and K-feldspar in a granodiorite pluton [53, 54]. Magmatic temperatures were estimated from geothermometry based on the solubility of zircon and monazite in the magma [44, 50]. Application of these geothermometers yielded temperatures of 680 to ~780 °C, respectively, for the monzonite, and ~675 to 760 °C, respectively for the granodiorite [37, 38]. The higher temperatures from the zircon geothermometer can be attributed to the fact that zircon is one of the earliest minerals to crystallize, i.e., these temperatures are close to that of the liquidus. Thus in summary, the above data suggest that the monzonitic and dioritic magmas in the Sungun stock crystallized over a temperature interval 675 to 780 °C and at a pressure of 500 bars.

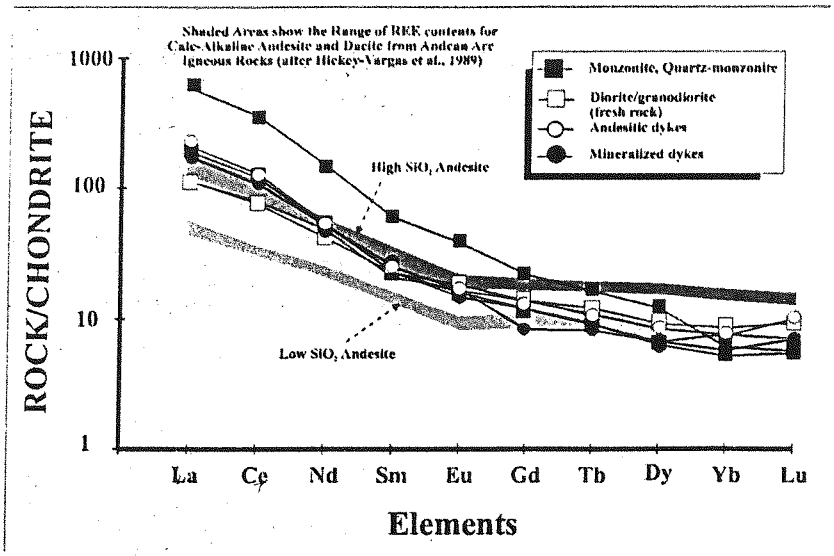

Figure (6) Chondrite-normalized REE plots of selected samples from different rock suites in the Sungun porphyry copper deposit. The rocks display a strong LREE enrichment ($La/Yb_{(N)} > 30$) and lack a Eu anomaly (see the text for discussion). Also shown on the diagram are fields for Andean calc-alkaline rocks [26].

Geochemical Evolution

Depletion of Fe, Ca, Mg, Sr, Y, Mn and Ni and enrichment of K, Na and Rb from monzonite/quartz-monzonite to diorite/granodiorite are consistent with early fractionation of pyroxene (?), hornblende, and calcic plagioclase, and later crystallization of biotite, albite, muscovite and K-feldspar. This evolution is also supported by the REE profiles in which diorite/granodiorite is HREE-enriched relative to monzonite/quartz-monzonite, but LREE-depleted. An unusual feature of the REE profiles, however, is the lack of a Eu anomaly. Normally, a negative Eu anomaly develops with magma evolution due to fractional crystallization of early, more calcic plagioclase [17]. However, at high fO_2 conditions, Eu will be present mainly as Eu^{+3} and therefore very little Eu^{+2} may be available for incorporation in plagioclase. This may be the explanation for the lack of a Eu anomaly in the Sungun stock.

Based on the previous arguments, and the field relationships between the monzonite and granodiorite, we propose, as a working hypothesis, that diorite/granodiorite and monzonite/quartz-monzonite represent less and more evolved batches of a calc-alkaline magma. It is possible to determine the extent of fractionation of a magma from the changing concentration of incompatible trace elements relative to compatible trace elements. In the case of rocks that have been subjected to alteration, it is important that the trace elements are also immobile, i.e., that except for overall mass gain or loss, any changes in trace element concentration will be due to fractionation. The latter will be evident as distributions with negative trends, and the overall mass gains and losses as deviations from the fractionation trends along lines that pass through the origin [28, 29].

The Y is used to represent the compatible trace element and Zr and Nb as alternative incompatible trace elements. Other potentially compatible elements yielded appreciable scatter and were therefore not considered further. The plots of Nb vs Y and Zr vs Y are presented in Figure 7. Also shown on this diagram are fractionation curves representing polynomial least squares fits through the data and dashed lines towards and away from the origin to show the directions of mass gains and losses, respectively. These diagrams confirm the earlier conclusion that diorite/granodiorite is the first suite and less evolved than monzonite/quartz-monzonite. They also suggest that even the least altered rocks have undergone some mass change. In order to quantitatively evaluate the degree of fractionation, it is necessary to first project the composition of each sample to the fractionation curve along lines of mass change (through the origin) and then select the least evolved sample (highest Y and lowest Zr content) to represent the parent magma. We took the latter to be sample 58-71 which has a projected initial concentration of 22 ppm Y, 97 ppm Zr or 23 ppm Y and 8 ppm Nb (Figs. 7a and b). With fractionation, the projected Zr content of the diorite/granodiorite ranged up to 110 ppm and the Nb content up to 12 ppm. Projected ranges for these elements in the more evolved monzonite/quartz-monzonite were 113 to 140 ppm and 13 to 21 ppm, respectivelly. The degree of fractional crystallization was calculated using the following Raleigh fractionation equation of [45]:

$$C_i^P = (1\text{-}X)\, C_i^D + X.(KD_i).C_i^{Crystal} * 100 \quad (1)$$

where C_i is the concentration of element i (e.g., Zr) in the parental rock P, D is the daughter rock, X is the degree of fractional crystallization, and KD_i is the partition coefficient for the i_{th} element between rock (crystal) and magma. The calculated degree of fractional crystallization, is between 15 and 22 % using the data for Zr (KD from 39 and Crecraft, 1985) and 17 to 24 % using the data for Nb (KD from [48].

Conclusion

The Sungun deposit is a composite stock, emplaced at a paleo-depth of ~2000 m, at temperatures ranging between 670 and 780 °C, and comprising early monzonite/quartz-monzonite and a later diorite/granodiorite phase. The parental magma was a medium to high K andesite or diorite similar in composition to syncollisional calc-alkaline magmas generated in continental arc settings. The presence of hydrous mineral like hornblende in the freshest diorite/granodiorite indicate that the corresponding magma initially contained >3 wt percent H_2O (wet magma). The high level emplacement of this magma, led to its saturation with water and the exsolution of fluids at an early stage of crystallization (which is characterized by the replacement of early hornblende with biotite), and subsequently Mo and then Cu mineralization in the stock [22, 23].

The Harker diagrams drawn for the major igneous suites display trends for compatible and incompatible major and trace elements which are consistent with fractional crystallization. Negative trends for Ca, Mg and Mn and positive trends of K, Na and Rb with increasing SiO_2 and the mineralogy of the intrusive suggest that a parental magma of diorite/granodiorite composition evolved by fractional crystallization of hornblende and Ca-plagioclase. The conclusion that the major intrusive suites evolved by fractional crystallization is supported by the behaviour of the immobile trace elements, Y, Zr and Nb. The degree of fractionation was estimated using a Rayleigh fractionation equation which related the concentration of Zr, Nb and Y in the least altered sample to their concentrations in progressively more evolved samples. The results of these calculations indicated that the compositions of the various rock types can be explained by up to 24 % fractionation of a diorite magma to produce the more evolved monzonite/quartz-monzonite suite.

Table (1) Electron Microprobe Analyses of Amphiboles in the Sungun Granodiorite.

Sample no.	1	2	3	4	5	6	7	8	9	10	11	12	13	14
Dril-core no.	23-158	23-158	23-158	23-158	23-158	23-158	23-158	23-158	23-158	23-158	23-158	23-158	23-158	23-158
Type [1]	Frs	Frs	Frs	Frs	Frs	Frs	Frs	Frs	Frs	Frs	Frs	Frs	Frs	Frs
SiO_2 (wt %)	48.88	46.99	45.89	46.82	47.16	47.01	46.76	47.77	47.09	47.19	45.88	48.01	47.05	46.52
TiO_2	1.18	1.45	1.50	1.34	1.28	1.43	1.33	1.12	1.11	1.20	1.36	1.13	1.25	1.31
Al_2O_3	6.29	7.10	7.78	7.24	6.81	7.22	7.11	7.04	7.00	6.83	7.84	6.71	7.37	7.34
FeO^2	11.88	12.50	13.36	13.08	13.08	13.29	13.23	12.60	12.86	12.97	13.55	13.12	13.18	13.01
MnO	0.46	0.43	0.44	0.47	0.43	0.44	0.47	0.46	0.40	0.41	0.42	0.46	0.44	0.45
MgO	16.43	15.46	15.00	15.38	15.30	15.06	15.10	15.66	15.36	15.63	14.68	15.52	15.20	15.21
CaO	11.27	11.21	11.27	11.48	11.30	11.39	11.27	11.39	11.34	11.21	11.41	11.39	11.39	11.22
Na_2O	1.33	1.85	1.57	1.51	1.67	1.50	1.55	1.43	1.68	1.52	1.78	1.48	1.49	1.68
K_2O	0.39	0.85	0.63	0.57	0.70	0.54	0.52	0.52	0.65	0.54	0.82	0.54	0.59	0.61
F	0.11	0.14	0.06	0.14	0.21	0.17	0.07	0.17	0.05	0.07	0.19	0.06	0.14	0.09
Cl	0.08	0.39	0.10	0.10	0.33	0.08	0.09	0.08	0.36	0.11	0.31	0.14	0.08	0.20
Total	98.28	98.37	97.58	98.12	98.26	98.11	97.48	98.22	97.90	97.66	98.23	98.54	98.18	97.63
No. of atoms based on 24 O														
Si	7.35	7.14	7.06	7.14	7.17	7.16	7.18	7.23	7.19	7.22	7.02	7.27	7.16	7.13
Ti	0.13	0.17	0.17	0.15	0.15	0.16	0.15	0.13	0.13	0.14	0.16	0.13	0.14	0.15
Al	1.12	1.27	1.41	1.30	1.22	1.30	1.29	1.26	1.26	1.23	1.42	1.20	1.32	1.33
Fe	1.50	1.59	1.72	1.67	1.66	1.69	1.70	1.60	1.64	1.66	1.74	1.66	1.68	1.67
Mn	0.06	0.06	0.06	0.06	0.06	0.06	0.06	0.06	0.05	0.05	0.05	0.06	0.06	0.06
Mg	3.68	3.50	3.44	3.49	3.47	3.42	3.46	3.54	3.50	3.56	3.35	3.50	3.45	3.48
Ca	1.82	1.82	1.86	1.87	1.84	1.86	1.85	1.85	1.86	1.84	1.87	1.85	1.86	1.84
Na	0.39	0.55	0.47	0.45	0.49	0.44	0.46	0.42	0.50	0.45	0.53	0.43	0.44	0.50
K	0.07	0.16	0.12	0.11	0.14	0.11	0.10	0.10	0.13	0.11	0.16	0.11	0.12	0.12
F	0.05	0.07	0.03	0.07	0.10	0.08	0.03	0.08	0.02	0.03	0.09	0.03	0.07	0.04
Cl	0.02	0.10	0.03	0.03	0.09	0.02	0.02	0.02	0.09	0.03	0.08	0.04	0.02	0.05
F/(F+Cl)	0.70	0.40	0.51	0.72	0.54	0.79	0.59	0.81	0.19	0.54	0.54	0.45	0.76	0.44
Fe/(Fe+Mg)	0.29	0.31	0.33	0.32	0.32	0.33	0.33	0.31	0.32	0.32	0.34	0.32	0.33	0.32

[1] Frs = fresh rock

[2] FeO = total Fe

Table (1) Cont'd, Electron Microprobe Analysis of Feldspars from Sungun Porphyry Copper Deposit.

Sample no.	1	2	3	4	5	6	7	8	9	10	11	12	13
Dril-core no.	33-437	33-437	33-437	33-437	33-437	33-437	33-437	33-437	33-354	33-354	33-354	33-354	33-354
Stage	K	K	K	K	K	K	K	K	K-Trn	K-Trn	K-Trn	K-Trn	K-Trn
SiO2	66.74	62.93	64.37	63.74	64.68	69.18	63.99	64.26	64.49	67.51	64.43	64.24	65.59
Al2O3	17.64	19.79	18.53	18.71	18.51	19.18	18.69	18.48	18.72	19.08	18.47	18.54	18.92
FeO	0.03	1.28	0.06	0.08	0.12	0.13	0.10	0.07	0.09	0.09	0.09	0.07	0.22
MgO	0.00	0.02	0.01	0.00	0.00	0.00	0.00	0.00	0.00	0.01	0.01	0.00	0.00
CaO	0.01	0.05	0.01	0.06	0.10	0.13	0.06	0.03	0.42	0.38	0.13	0.09	0.65
Na2O	0.39	1.85	0.80	1.28	2.02	1.62	1.31	0.92	1.64	1.32	1.27	1.20	2.72
K2O	15.84	13.05	16.19	15.33	13.61	9.69	14.95	15.56	14.52	11.60	15.06	15.36	13.33
BaO	0.99	0.71	0.85	1.08	1.34	1.32	1.05	1.40	1.00	1.05	0.92	0.74	0.14
Total	101.64	99.67	100.82	100.28	100.39	101.23	100.14	100.72	100.87	101.03	100.37	100.24	101.57
No. of atoms based on 8 O													
Si	3.04	2.92	2.98	2.96	2.98	3.06	2.97	2.98	2.97	3.03	2.98	2.98	2.97
Al	0.95	1.08	1.01	1.02	1.00	0.98	1.02	1.01	1.01	1.01	1.00	1.01	1.01
Fe	0.00	0.05	0.00	0.00	0.00	0.00	0.00	0.00	0.00	0.00	0.00	0.00	0.00
Mg	0.00	0.00	0.00	0.00	0.00	0.00	0.00	0.00	0.00	0.00	0.00	0.00	0.00
Ca	0.00	0.00	0.00	0.00	0.00	0.00	0.00	0.00	0.02	0.02	0.01	0.01	0.03
Na	0.04	0.17	0.07	0.12	0.18	0.14	0.12	0.08	0.15	0.12	0.10	0.11	0.24
K	0.94	0.77	0.96	0.91	0.80	0.55	0.89	0.92	0.85	0.66	0.89	0.91	0.77
Ba	0.02	0.01	0.02	0.02	0.02	0.02	0.02	0.03	0.02	0.02	0.02	0.01	0.00
Sum	4.99	5.00	5.04	5.03	4.98	4.75	5.02	5.02	5.02	4.85	5.00	5.03	5.02
sum of cations	0.98	0.94	1.03	1.03	0.98	0.69	1.01	1.00	1.02	0.80	1.00	1.03	1.04
Or	95.92	81.91	93.20	88.35	81.63	79.71	88.12	92.00	83.33	83.31	89.00	88.35	74.04
Ab	4.08	18.09	6.80	11.65	18.37	20.29	11.88	8.00	14.71	14.43	10.00	10.68	23.08
An	0.00	0.00	0.00	0.00	0.00	0.00	0.00	0.00	1.96	2.26	1.00	0.97	2.88
Or/(Or+Ab+An)	0.96	0.82	0.93	0.88	0.82	0.80	0.88	0.92	0.83	0.83	0.89	0.88	0.74

[1] Frs = fresh rock, K = potassic zone, K-Trn = potassic-transition zone, Phc = phyllic

17

Feldspars (cont.)

Sample no.	14	15	16	17	18	19	20	21	22	23	24	25	26	27
Dril-core no.	33-354	25-444	25-444	25-444	25-444	25-444	25-444	25-444	25-444	25-444	25-444	25-421	25-421	25-421
Stage	K-Trn	K	K	K	K	K	K	K	K	K	K	K	K	K
SiO2	65.08	64.60	64.95	64.81	64.41	64.86	65.72	64.43	64.95	65.92	64.68	66.72	65.09	64.79
Al2O3	18.31	18.59	18.73	18.41	18.34	18.43	17.89	18.70	18.39	17.71	18.31	17.79	18.26	18.52
FeO	0.07	0.09	0.04	0.09	0.09	0.05	0.04	0.09	0.08	0.20	0.07	0.06	0.08	0.05
MgO	0.00	0.00	0.00	0.00	0.00	0.00	0.00	0.00	0.00	0.01	0.00	0.00	0.00	0.00
CaO	0.00	0.01	0.02	0.03	0.05	0.00	0.00	0.18	0.08	0.08	0.05	0.06	0.00	0.04
Na2O	0.95	1.03	1.06	1.10	1.08	0.88	0.12	1.92	1.30	0.95	1.02	1.35	0.89	1.22
K2O	15.87	15.68	15.73	15.48	15.57	16.00	17.44	13.84	15.10	15.68	15.86	14.73	16.03	15.40
BaO	0.53	0.85	0.99	0.85	1.02	0.88	0.16	1.33	0.98	0.32	0.65	0.98	0.64	0.75
Total	100.80	100.85	101.52	100.78	100.56	101.10	101.37	100.49	100.89	100.87	100.63	101.70	100.98	100.76
No. of atoms based on 8 O														
Si	2.99	2.98	2.98	2.99	2.98	2.99	3.01	2.97	2.99	3.02	2.99	3.03	2.99	2.98
Al	0.99	1.01	1.01	0.98	1.00	0.98	0.96	1.01	1.00	0.96	0.99	0.99	0.98	1.00
Fe	0.00	0.00	0.00	0.00	0.00	0.00	0.00	0.00	0.00	0.01	0.00	0.00	0.00	0.00
Mg	0.00	0.00	0.00	0.00	0.00	0.00	0,00	0.00	0.00	0.00	0.00	0.00	0.00	0.00
Ca	0.00	0.00	0.00	0.00	0.00	0.00	0.00	0.00	0.00	0.00	0.00	0.00	0.00	0.00
Na	0.10	0.10	0.09	0.09	0.10	0.07	0.00	0.01	0.00	0.00	0.00	0.00	0.00	0.00
K	0.92	0.92	0.92	0.92	0.92	0.94	0.01	0.17	0.12	0.08	0.09	0.12	0.10	0.11
Ba	0.01	0.02	0.02	0.02	0.02	0.02	1.02	0.82	0.89	0.92	0.93	0.84	0.92	0.90
Sum	5.01	5.03	5.02	5.00	5.02	5.00	0.00	0.02	0.02	0.01	0.01	0.02	0.01	0.01
							5.00	5.00	5.02	5.00	5.01	5.00	5.00	5.00
sum of cations	1.02	1.02	1.01	1.01	1.02	1.01	1.03	1.00	1.01	1.00	1.02	0.96	1.02	1.01
Or	90.20	90.20	91.09	91.09	90.20	93.07	99.03	82.00	88.12	92.00	91.18	87.50	90.20	89.11
Ab	9.80	9.80	8.91	8.91	9.80	6.93	0.97	17.00	11.88	8.00	8.82	12.50	9.80	10.89
An	0.00	0.00	0.00	0.00	0.00	0.00	0.00	1.00	0.00	0.00	0.00	0.00	0.00	0.00
Or/(Or+Ab+An)	0.90	0.90	0.91	0.91	0.90	0.93	0.99	0.82	0.88	0.92	0.91	0.88	0.90	0.89

Table (2) Major (wt %) and Trace Element (ppm) Analyses of Representative Fresh and Altered Rocks from the Sungun Porphyry Copper Deposit

Granodiorite																	
Sample no.	58-140	58-146	58-71	30-149	30-138	70-141	34-282	70-175	30-168	21-32	26-277	44-345	44-371	44-409	44-429
Type	Frs	Frs	Frs	Frs	Frs	Frs	Frs	Frs	K	K	K	K	K	K	K
SiO_2	54.15	49.21	56.04	60.53	60.54	59.02	61.68	58.84	61.89	57.76	64.8	64.12	65.92	59.07	62.92
TiO_2	0.8	0.83	0.73	0.57	0.58	0.59	0.57	0.62	0.58	0.47	0.68	0.48	0.49	0.58	0.56
Al_2O_3	16.31	16.78	16.41	15.88	15.96	15.74	16.02	16.12	15.89	14.42	16.45	15.57	15.56	15.43	15.85
Fe_2O_3[1]	6.93	7.2	6.34	4.94	4.91	5.1	4.94	5.51	3.52	5.04	1.27	2.12	1.71	4.07	1.7
MnO	0.13	0.13	0.12	0.1	0.1	0.09	0.09	0.11	0.08	0.07	0.03	0.04	0.01	0.09	0.03
MgO	4.25	4.28	3.73	2.56	2.61	2.59	2.52	3.52	2.06	2.27	1.13	1.43	1.35	2.32	1.67
CaO	6.28	7	6.39	4.98	4.66	5.06	4.64	5.11	4.38	3.77	2.04	2.35	1.85	4.46	2.98
Na_2O	3.83	3.32	3.55	4.04	3.96	3.57	3.85	4.14	1.03	1.71	0.23	1.87	0.98	3.38	0.21
K_2O	2.44	3.7	2.32	2.48	2.63	2.12	2.58	2.38	3.76	6.28	6.32	5.95	6.94	2.87	5.71
P2O5	0.24	0.25	0.23	0.24	0.24	0.25	0.24	0.23	0.25	0.25	0.35	0.26	0.26	0.24	0.3
L.O.I.	5.53	7.85	4.71	4.14	4.37	6.16	3.63	3.92	6.54	5.38	5.07	3.47	3.56	7.76	6.66
Total	100.99	100.72	100.67	100.56	100.56	100.43	100.9	100.65	99.98	98.06	99.66	99.33	99.74	100.37	99.35
Ba	748	1138	684	835	833	787	944	857	175	2044	1305	1059	1629	558	1216
Ce	64	57	61	80	53	59	58	51	87	192	110	130	67	48	132
Co	13	25	24	21	12	15	19	14	10	16	13	19	24	20	18
Cr_2O_3	56	61	57	49	56	47	64	131	48	44	123	52	55	47	76
Cu	98	56	81	98	64	201	224	127	50	3327	9080	13050	7845	196	5160
Ni	49	50	42	22	27	29	25	41	29	35	17	15	26	23	40
Sc	23	26	26	18	19	19	16	27	14	11	5	6	2	11	4
V	154	154	141	85	95	98	99	110	84	61	87	66	59	89	79
Zn	59	60	58	53	50	55	52	49	50	640	1640	2353	1420	122	962
Ga	18	17	18	17	17	17	17	17	17	17	12	14	13	16	16
Nb	7	13	5	10	9	13	10	9	16	17	18	19	18	11	20
Pb	14	24	17	16	14	11	13	12	13	21	13	28	9	11	11
Rb	49	89	50	58	64	56	56	52	98	118	100	118	125	81	112
Sr	785	461	1334	699	664	210	715	673	283	418	633	1035	849	326	951
Th	8	1	10	9	9	7	10	8	11	22	11	21	17	2	20

U	0	2	0	0	0	0	0	0	0	D/L	D/L	D/L	D/L	D/L	D/L
Y	22	19	20	18	18	19	17	19	16	18	12	8	9	15	11
Zr	111	115	96	104	99	115	105	103	119	116	168	118	130	105	120

[1] Total Fe as Fe_2O_3, D/L = Below detection limit,

Frs = Fresh, K = Potassic alteration zone, Trn = transition alteration zone,, Phc = Phyllic alteration zone,

Arg = argillic alteration zone, L.O.I = Loss on ignition,

* = Rock analyses from Mehrpartou, 1993

(Cont'd)

Granodiorite														
Sample no.	25-122	29-195	25-517	34-163	25-453	7-150.6	25-522	30-200	25-239	25-275	33-281	26-237	25-371	26-239
Type	Trn	K	K	K	K	K	Trn	Trn	Phc	Phc	Phc	Phc	Phc	Phc
SiO_2	61.66	64.47	62.94	63.31	61.51	58.88	61.98	61.66	71.09	69.09	57.25	68.80	68.01	67.38
TiO_2	0.51	0.49	0.46	0.76	0.48	0.49	0.49	0.47	0.64	0.58	0.56	0.42	0.51	0.51
Al_2O_3	15.92	16	15.02	15.21	15.86	15.98	15.88	15.91	15.98	15.69	15.63	12.99	15.88	14.21
Fe_2O_3[1]	3.88	3.36	4.58	2.97	4.02	4.51	3.44	3.91	2.40	2.26	4.83	1.62	2.68	2.79
MnO	0.14	0.05	0.02	0.05	0.04	0.02	0.13	0.13	0.02	0.01	0.02	0.01	0.05	0.10
MgO	2.04	1.87	1.29	3.45	2.36	1.35	1.76	1.85	1.59	1.03	1.54	1.50	3.41	2.81
CaO	4.14	3.12	2.56	4.77	2.72	2.65	4.19	3.25	1.69	1.55	3.57	2.51	4.23	3.54
Na_2O	3.54	4.49	2.45	4.61	3.87	2.46	3.48	3.11	0.08	2.23	1.08	0.99	0.91	1.87
K_2O	3.07	4.02	4.70	4.50	4.03	4.60	3.85	3.96	4.48	4.78	4.00	4.88	3.56	3.22
P2O5	0.25	0.25	0.24	0.51	0.25	0.25	0.26	0.22	0.33	0.28	0.30	0.20	0.12	0.20
L.O.I.	5.85	2.43	4.59	3.81	2.85	5.27	5.14	5.68	2.12	3.61	7.05	4.18	2.56	3.21
Total	100.75	100.73	99.24	99.38	99.74	99.13	100.06	99.53	100.42	99.53	98.82	99.24	101.80	99.84
Ba	981	1219	1266	667	1497	1288	1203	863	485	739	1105	1264	657	853
Ce	81	111	78	74	123	79	93	75	81	68	75	63	74	43
Co	10	1	18	11	9	3	12	10	20	0	45	18	12	11
Cr_2O_3	40	83	63	269	132	63	46	83	111	40	105	80	279	26
Cu	36	140	2312	615	619	1826	43	87	691	872	2566	8257	715	467
Ni	44	36	24	91	91	33	25	43	67	14	73	84	93	47
Sc	13	9	15	19	15	10	15	13	11	11	10	3	12	13
V	74	65	61	95	71	61	70	66	106	62	80	51	18	54
Zn	115	25	21	42	60	29	61	62	17	6	516	1494	95	85

Ga	17	17	18	19	18	19	17	18	17	17	18	11	39	10
Nb	15	15	10	22	15	17	14	16	21	13	19	15	21	23
Pb	36	16	14	14	28	20	12	50	13	14	14	11	22	17
Rb	77	76	102	61	74	102	98	112	103	90	111	91	61	63
Sr	352	900	1194	296	867	365	732	430	66	69	292	961	271	569
Th	13	23	27	13	27	26	17	18	8	20	19	16	13	16
U	2	2	6	4	5	10	5	5	1	0	D/L	D/L	4	3
Y	14	11	12	15	12	13	13	13	12	4	13	7	14	11
Zr	114	112	108	151	109	112	117	110	137	133	158	89	151	149

(Cont'd)

						Andesitic Dykes									
25-134	Sample no.	25-171	25-213	34-137	34-241	25-167	30-283	44-413	30-102	38-183	34-445	25-395	30-227	25-394	38-167
Arg	Type	Arg	Arg	Arg	Arg	Frs	Frs	Frs	Frs	Frs	Frs	Frs	Frs	Frs	Frs
63.71	SiO_2	64.89	70.48	68.18	71.12	56.61	58.25	58.71	58.01	57.71	59.91	58.36	56.71	57.81	56.24
0.40	TiO_2	0.52	0.42	0.64	0.50	0.68	0.66	0.65	0.65	0.65	0.71	0.71	0.72	0.69	0.77
18.61	Al_2O_3	19.30	18.31	17.54	16.53	15.51	15.98	15.79	15.91	15.49	16.11	16.11	15.59	15.99	17.19
0.10	$Fe_2O_3{}^1$	4.32	4.20	3.11	2.98	5.41	5.69	5.67	5.77	6.01	6.01	5.89	5.39	5.89	5.83
0.01	MnO	0.02	0.19	0.01	0.01	0.08	0.09	0.08	0.08	0.09	0.09	0.09	0.1	0.1	0.13
0.67	MgO	1.12	0.31	1.12	0.73	2.67	3.7	3.8	3.8	3.31	4.01	4.23	2.59	4.22	3.99
1.00	CaO	0.43	0.67	0.51	0.12	6.97	6.21	5.71	6.01	5.42	5.41	5.65	6.98	5.64	5.91
0.64	Na_2O	4.21	0.17	0.11	1.00	3.12	3.51	3.51	3.52	3.4	4.01	4	3.11	3.99	3.68
4.93	K_2O	1.21	0.10	4.21	1.53	2.1	2.3	2.3	2.41	2.52	2.39	2.35	2.07	2.32	4.7
0.05	P2O5	0.32	0.30	0.08	0.17	0.28	0.26	0.27	0.25	0.26	0.25	0.26	0.25	0.25	0.27
6.11	L.O.I.	4.37	5.23	4.10	6.10	5.53	4.23	3.57	3.67	5.67	1.54	3.25	5.91	3.21	2.13
95.63	Total	100.71	100.38	99.61	100.79	98.96	100.88	100.06	100.08	100.53	100.44	100.9	99.42	100.11	100.84
412	Ba	532	894	971	647	1241	708	710	681	840	701	733	1298	731	1922
43	Ce	51	43	121	64	23	34	41	34	63	22	23	35	31	45
12	Co	11	10	18	13	1	3	1	7	2	1	4	3	5	0
76	Cr_2O_3	68	101	78	54	81	104	79	101	105	79	102	83	101	61
12	Cu	84	451	59	84	33	41	41	44	41	39	32	55	41	30
															21

67	Ni	34	71	13	26	51	45	37	41	33	44	43	39	51	24
14	Sc	15	18	21	3	1	1	2	1	1	1	2	2	4	1
63	V	68	89	19	132	114	119	91	117	108	140	139	109	140	11[illegible]
56	Zn	62	78	90	45	63	55	52	53	59	55	63	66	63	97
17	Ga	16	15	18	15	18	10.5	12.1	11.1	17	14	15	16	15	16
19	Nb	12	20	14	12	12	11	13	12	11	13	11	13	11	11
23	Pb	43	11	18	52	24	13	10	10	13	20	12	10	13	17
71	Rb	89	84	98	109	61	55	81	49	61	59	58	51	58	10[illegible]
56	Sr	74	145	39	98	1521	1989	847	787	601	849	759	1530	781	52[illegible]
18	Th	14	19	23	23	21	14	14.7	12	10	15	7	11	12	11
3	U	7	3	2	8	D/L	D/L	D/L	D/L	D/L	D/L	D/L	D/L	D/L	D.L
9	Y	9	6	11	12	15	16.5	18.5	11	9	17	12.1	14	15.2	14
135	Zr	79	141	171	150	133	123	121	121	117	120	110	121	114	128

Table (3) Neutron Activation Analyses of REE'S (ppm) from the Sungun Deposit.

Sample No.	25-522	34-163	33-281	44-409	30-168	21-32
Dril-core No.	25	34	33	44	30	21
Type [1]	Granodiorite (K)	Mineralized dykes (K)	Granodiorite (Frs)	Andesitic dykes (Phc)	Mineralized dykes (Phc)	Monzonite/ qz-monzonite (Frs)
La (ppm)	46.7	64.5	51.0	27.4	40.2	139.0
Ce	76.6	106.0	81.0	50.0	67.2	228.0
Nd	24.9	34.0	25.4	23.0	23.8	72.0
Sm	3.6	4.4	3.5	3.1	3.8	9.3
Eu	0.9	1.2	0.9	1.0	1.0	2.2
Gd	2.4	1.9	2.5	1.7	2.8	4.4
Tb	0.3	0.3	0.3	0.3	0.4	0.6
Dy	1.6	1.6	1.7	1.6	2.1	3.1
Yb	0.9	0.9	0.9	1.3	1.2	1.0
Lu	0.1	0.1	0.2	0.2	0.3	0.1

[1] Frs = fresh rock, K = potassic alteration zone, Phc = phyllic alteration zone

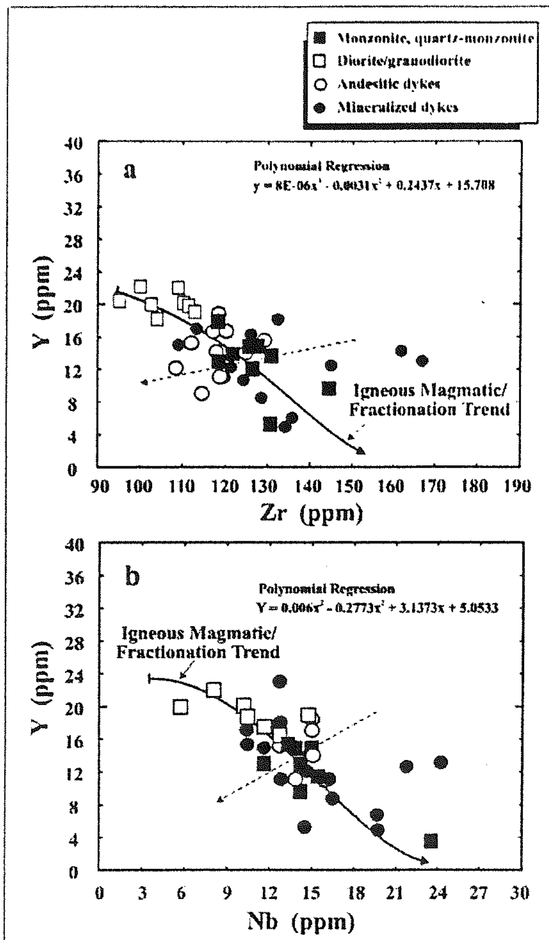

Figure (7) Diagram showing the concentration of a. Y vs. Zr, and b. Y vs. Nb. Fractional crystallization trends are indicated by curves representing least square lines. Samples off the curve are projected onto the curve by straight lines (dashed arrow) projected through the origin. Their deviations indicate the extent of mass gain (negative or positive deviations from the fractional crystallization curve) mass loss. The fractional crystallization value of minimum of 15 to maximum of 22, to produce quartz-monzonite/monzonite from granodioritic magma, has been calculated using the concentration of Y and Zr, based on the KD of Zr in felsic magmas. See text for more information.

References

[1] **Berberian, M., 1976,** Contribution to the Seismotectonics of Iran (part II). *Geological survey of iran. v. 39, 518p, 5 maps, 259 figures.*

[2] **Berberian, M., 1983,** The southern Caspian: A compressional depression floored by a trapped, modified oceanic crust: *Can. J. Earth Sci. v. 20, p. 163-183.*

[3] **Berberian, M., and King, G. C., 1981,** Towards a paleogeography and tectonic evolution of Iran: Can. J. Earth Sci. v. 18, p. 210-265.Bloom, M. S., 1981, Chemistry of inclusion fluids: Stockwork Molybdenum deposits from Questa, New Mexico, and Hudson bay mountain and Endako, British Columbia: *Economic GEOLOGY, v. 76, p. 1906-1920.*

[4] **Burnham, C. W., 1979,** Magmas and hydrothermal fluids: in Geochemistry of Hydrothermal ore deposits, H. L. Barnes, *Jon Wiley & sons, Inc., p. 71-136.*

[5] **Carmichael, I. S. E., and Eugster, H. P., 1987,** Thermodynamic modelling of geological materials: minerals, fluids and melts: *Reviews in mineralogy., v. 17, 499pp.*

[6] **Carmichael, I. S. E., Turner, F. J., and Verhoogen, J., 1974,** Igneous petrology: New York, *McGraw-Hill, 739p.*

[7] **Carten, R. B., 1986,** Sodium-calcium metasomatism: chemical, temporal, and spatial relationships at the Yerington, Nevada, porphyry copper deposit: *Economic geology, v. 81, p. 1495-1519.*

[8] **Cox, D. P., Schemidt, R. G., Vine, J. D., Kirkemo, H., Tourtelot, E., and Fleischer, M., 1973b,** Copper in Brobst, D. A., Pratt, W. P., eds., United states mineral resources: U. S., *Geological survey professional paper, v. 820, p. 163-190.*

[9] **Cox, K. G., Bell, J. D., and Pankhurst, R. J., 1979,** The interpretation of Igneous Rocks, *George Allen and Unwin, London.*

[10] **Dilles, J. H., 1987,** Petrology of the Yerington Batholith, Nevada: Evidence for Evolution of Porphyry Copper Ore Fluids: *Economic geology, qv. 82, p. 1750-1789.*

[11] **Eastoe, C. G.,and Eadington, P. J., 1986,** High-temperature fluid inclusions and the role of the biotite granodiorite in mineralization at the Punguna porphyry copper deposit, Bougainville, Papua New Guinea: Economic geology, v. 81, p. 478-483.

[12] **Eastoe, C. G., 1978,** A fluid inclusion study of the Panguna porphyry copper deposit, Bougainville, PaPua New Guinea: *Economic geology, v. 73, p. 721-748.*

[13] **Ewart, A., 1982,** The mineralogy and petrology of Tertiary-recent orogenic volcanic rocks: with special reference to the andesitic-basaltic compositional range, in Thorpe, R. S., ed., andesites: orogenic andesites and related rocks: *Chichester, Jone Wiley and Sons, p. 25-95.*

[14] **Gill, J. B., 1978,** The role of trace element partition coefficients in models of andesite genesis: *Geochimica et cosmochimica acta, v. 42, p. 709-724.*

[15] **Gill, J. B., 1981,** Orogenic andesites and plate tectonics: *New York, Springer-Verlag, 390p.*

[16] **Hassanzadeh, J., 1993,** Metallogenic and tectono-magmatic events in SE sector of the Cenozoic active continental margin of central Iran (Shahre-Babak, Kerman Province). *pH. D. thesis, University of California, Los Angeles, 204p.*

[17] **Henderson, P., 1984,** Rare Earth Element geochemistry, *Elsevier, 510p.*

[18] **Hezarkhani A, (2003),** Hydrothermal Evolution in the Raigan Porphyry Copper System Based on Fluid Inclusion studies, (Kerman, Iran): The Path to an Uneconomic Deposit. *Amirkabir Journal of Science and Technology, v. 15, No. 57-D, (Basic Science and Applied Engineering), Winter 2004, p. 74-84.*

[19] **Hezarkhani, A (2002),** Specific Physico-Chemical Conditions (360 °C) for Chalcopyrite Dissolution/Deposition in the Sungun Porphyry Copper Deposit, Iran. *Amirkabir journal of science and technology, v. 13, no. 52, p. 668-687.*

[20] **Hezarkhani, A., Williams-Jones, A. E., and Gammons, C. H., (1999),** Factors controlling copper solubility and chalcopyrite deposition in the Sungun porphyry copper deposit, Iran. *Mineralium deposita, vol. 34, pp. 770-783.*

[21] **Hezarkhani, A., and Williams-Jones, A. E., (1998),** Controls of alteration and mineralization in the Sungun Porphyry Copper Deposit, Iran: Evidence from fluid inclusions and stable isotopes. *Economic Geology. vol. 93, pp. 651-670.*

[22] **Hezarkhani, A, Williams-Jones, A. E., and Gammons, C., (1997),** Copper solubility and deposition conditions in the potassic and phyllic alteration zones, at the Sungun Porphyry Copper Deposit, Iran. *Geol. Assoc. Canada-Mineralogical Assoc. Canada (GAC-MAC) Annual Meeting, Ottawa, v. 50, p. A-67.*

[23] **Hezarkhani, A, and Williams-Jones, A. E., (1996),** Physico-chemical controles of alteration and mineralization at the Sungun Porphyry Copper Deposit, Iran. *Geol. Assoc. Canada-Mineralogical Assoc. Canada (GAC-MAC) Annual Meeting, Winnipeg, v. 21, p. A-44.*

[24] **Hezarkhani, A. (1997),** Physicochemical Controls on Alteration and Copper Mineralization in the Sungun Porphyry Copper Deposit, *Iran, Ph.D. Thesis, McGill University, Canada, 281p.*

[25] **Hezarkhani, A. 1988,** Geology and petrology of the Kashan igneous rocks, from Ravand to Naragh; Central Iran: *M.S.C thesis, Tehran University, pp. 161.*

[26] **Hickey-Vargas, R., Moreno Roa, H., Escobar, L. L., and Frey, A. F., 1989,** Geochemical variations in Andean basaltic and silicic lavas from the Villarrica-Lanin volcanic chain (39.5°C): an evaluation of source heterogeneity, fractional crystallization and crustal assimilation, *Contributions to mineralogy and petrology, v. 103, p. 361-386.*

[27] **Lescuyer, J. L., Riou, R., Babakhani, A., Alavi Tehrani, N., Nogol, M. A., Dido, J., Gemain, Y. M., 1978,** Geological map of the Ahar area: *Geological survey of iran.*

[28] **MacLean, W. H., 1990,** Mass change calculations in altered series, *Mineralum deposita, v. 25, p. 44-49.*

[29] **MacLean, W. H., and Barrett, T. J.,** Lithogeochemical techniques using immobile elements, *Journal of geochemical exploration, v. 48, p. 109-133.*

[30] **Mason, D. R., 1978,** Compositional variations in ferromagnesian minerals from porphyry copper-generating and barren intrusions of the Western Highlands, Papua New Guinea; *Economic geology, v. 73, p. 878-890.*

[31] **Mason, D. R., 1978,** Composition Variation in Ferromagnesian minerals from porphyry copper-generating and barren intrusions of the Western Highlands, Papua New Guinea, *Economic geology, v. 73, p. 878-890.*

[32] **Mason, D. R., and McDonald, J. A., 1978,** Intrusive rocks and porphyry copper occurences of the Papua New Guinea-Solomon Islands region: *Economic geology, v.73, p. 857-877.*

[33] **McDonough, W. F., and Frey, F. A., 1989,** Rare earth elements in upper mantle rocks. *Mineralogical society of america. reviews in mineralogy.*

[34] **Mehrpartou, M., 1993,** Contributions to the geology, geochemistry, ore genesis and fluid inclusion investigations on Sungun Cu-Mo porphyry deposit, (North-West of Iran). *Ph.D thesis, Hamburg Univ. Hamburg, 245p.*

[35] **Miyashiro, A., 1974,** Volcanic rock series in island arcs and active continental margins, *Americal Journal of Science, v. 274, p. 321-355.*

[36] **Miyashiro, A., 1978,** Nature of alkalic volcanic rock series: *Contrib. mineral. petrol., v. 66, p. 91-104.*

[37] **Mulja, T, Williams-Jones, A. E., Wood, S. A., and Boily, M., 1995,** The rare-element-enriched monzogranite-pegmatite-quartz vein systems in the Preissac-Lacorne batholith, Quebec. *I. geology and mineralogy: Canadian mineralogist, v. 33, p. 793-815.*

[38] **Mulja, T, Williams-Jones, A. E., Wood, S. A., and Boily, M., 1995,** The rare-element-enriched monzogranite-pegmatite-quartz vein systems in the Preissac-Lacorne batholith, Quebec. *II. geochemistry and petrogenesis: Canadian mineralogist, v. 33, p. 817-833*

[39] **Nash, W. P., and Crecraft, H. R., 1985,** Partition coefficients for trace elements in silicic magma, *Geochimica et cosmochimica acta, v. 49, p. 2309-2322.*

[40] **Papike, J. J., 1988,** Chemistry of the rock-forming silicates: multiple-chain, sheet, and framework structures: *Reviews of geophysics, v. 26, p. 407-444.*

[41] **Pearce, J. A., and Cann, J. R., 1973,** Tectonic setting of basic volcanic rocks determined using trace element analyses, *Earth and Planetary science letters, v. 19, p. 290-300.*

[42] **Pearce, J. A., Harris, N. B. W., and Tindle, A. G., 1984,** Trace element discrimination diagrams for the tectonic interpretation of granitic rocks, *Journal of Petrology, v. 25, p. 956-983.*

[43] **Pourhosseini, F., 1981,** Petrogenesis of Iranian plutons: a study of the Natanz and Bazman intrusive complexes: *Ph.D thesis, University of Cambridge, 315p.*

[44] **Rapp, R. P., and Watson, E. B., 1986,** Monazite solubility and dissolution kinetics: implications for the thorium and light rare earth chemistry of felsic magmas: *Contribution to mineralogy and petrology. v. 94, p. 304-316.*

[45] **Shaw, D. M., 1979,** Trace element models. *Physics and chemistry of the earth. v. 11, p. 577-586.*

[46] **Stöcklin, J., 1977,** Structural correlation of the Alpine ranges between Iran and Central Asia. *Mem. H. Aser. Soc. Geol. France, pp. 333-353.*

[47] **Stöcklin, J., and Setudenia, A. 1972,** Lexique Stratigraphique International Volume III ASIE Centre National De La Recherche Scientifique. *15, quai Anole-France, pp. 75, (Paris-VII).*

[48] **Sweeney, R. J., Green, D. H., and Sie, S. H., 1992,** Trace and minor element partitioning between garnet and amphibole and carbonatitic melt, *Earth planet science letters. v. 91, p. 1-14.*

[49] **Wall, V. L., Clemens, J. D., and Clarke, D. B., 1987,** Models for granotoid evolution and source composition.. *Jounal of Geology, v. 6, p. 731-749.*

[50] **Watson, E. B., and Harrison, T. M., 1983,** Zircon saturation revisited: temperature and composition effects in a variety of crustal magma types. *Earth planet science letters, v. 64, p. 295-304.*

[51] **Whitney, J. A., 1989,** Origin and evolution of silicic magmas: Ore deposition associated with magmas: *Reviews in economic geology, v. 4, p. 183-201.*

[52] **Whitney, J. A., 1988,** The origin of granite: The role and source of water in the evolution of granitic magmas: *Geological society of america bull., v. 100, p. 1886-1897.*

[53] **Whitney, J. A., 1975,** Vapour generation in a quartz monzonite magma: A synthetic model with application to porphyry copper deposits: *Economic geology, v. 70, p. 346-358.*

[54] **Whitney, J. A., and Stormer, J. C. 1985,** Mineralogy, petrology, and magmatic conditions from the Fish Canyon Tuff, central San Juan volcanic field, Colorado: *Journal of petrology, v. 26, pp. 726-762.*

[55] **Winchester, J. A., and Floyd, P. A., 1977,** Geochemical discrimination of different magma series and their differentiation products using immobile elements, *Chemical geology. v. 20, p. 325-343.*